17. Construct #412 is similar to #463 with two notable exceptions: There is only one α-globin gene in which CD59 is inserted at the start codon, and the α-globin promoter and LCR are replaced with a chick β-actin promoter. In the line of mice used in this report, expression was characterized on heart ECs but not RBCs. As for construct #528, it is a 70-kb genomic fragment that includes the complete CD59 gene, promoter, and flanking sequences. Expression was detected on ECs and RBCs. Expression on RBCs was lower than that observed in #463 and #506 mice.
18. Mouse hearts were removed and dissected into quarters to expose the linings of the chambers and rinsed in PBS. The heart fragments from two mice were digested in 5 ml of dispase [50 U/ml (Collaborative Biomedical Products, Bedford, MA)] for 30 min at 37°C in a shaking water bath. The resulting cell suspension was pelleted and washed three times in PBS. Cells (1×10^8) were stained for factor VIII (with FITC) (FL1) and for CD59 (with phycoerythrin) (FL2). Appropriate single-color and matched-isotype controls were also stained. Cells were analyzed on a Coulter Profile II cytometer by using a dual plot of forward scatter versus FL1 to gate the population of ECs. It was estimated that this population comprised approximately 5% of the cells analyzed (calculated without discrimination of the forward scatter). Gated cells were then analyzed on a dual-color plot of FL1 versus FL2.
19. Blood (~200 μl) was collected from transgenic and nontransgenic mice. Immediately after collection, a fraction enriched in polyadenylated RNA was isolated by Quick Prep (Pharmacia, Piscataway, NJ) according to the manufacture's protocol. Reverse transcriptase reactions were performed with the First-Strand cDNA Synthesis Kit (Pharmacia) according to the manufacture's protocol before PCR. Primers were used to amplify an 801–base pair (bp) fragment (after splicing) which extended from the first exon of CD59 to the second exon of α-globin from a nontransgenic bone marrow recipient, a representative bone marrow donor, and transgenic mice expressing constructs #412 and #506. The sequence of the CD59 primer was 5′-ATGGGAATCCAAGGAGGGT-3′, and the sequence of the α-globin primer was 5′-GCAAAGGTGCCCTTGAGG-3′. Primers were used that would amplify a 420-bp (after splicing) product extending from exon 1 to exon 4 from construct #528 mRNA. The sequences of these primers were (5′ primer) 5′-AGGCTGGAAGAGGATCTTGG-3′ and (3′ primer) 5′-TCTCCTGGTGTTGACT-TAGG-3′.
20. L. Y. Leong *et al.*, *Eur. J. Immunol.* **22**, 2825 (1992).
21. Mice were anesthetized with isoflurane or pentobarbital (50 mg per kilogram of body mass, administered intraperitoneally) and the chest opened. The heart was cooled with ice slush and explanted. The tip of a 22-guage angiocatheter was secured in the aortic root while the heart was maintained at 4°C. The Langendorff circuit consisted of a reservoir, a roller pump, and a column that provided 25 cm of perfusion pressure to the heart. Before suspending the heart from the circuit, the circuit was filled with IMDM with 50 mM Hepes (Gibco, Grand Island, NY) and allowed to equilibrate thermally and to a pH of 7.4. The perfusion fluid was oxygenated by bubbling O_2 (0.5 liter/min) into the reservoir and maintained at 38°C. The heart was suspended from the apparatus and the heart rate monitored. After 30 min of stabilization, 7 ml of medium was removed from the reservoir and 10 ml of 60% human plasma, diluted in IMDM, was added to yield a final concentration of 50% human plasma. The heart rate was monitored for 1 hour. Biopsies of the heart obtained at the conclusion of the procedure were prepared and stained as previously described (*13*).
22. S. Meri *et al.*, *Immunology* **71**, 1 (1990).
23. A. Vakeva *et al.*, *ibid.* **82**, 28 (1994).
24. M. R. Rifkin and F. R. Landsberger, *Proc. Natl. Acad. Sci. U.S.A.* **87**, 801 (1990).
25. E. J. Pearce, B. F. Hall, A. Sher, *J. Immunol.* **144**, 2751 (1990).
26. T. Kinoshita, *Immunol. Today* **12**, 291 (1991).
27. We would like to thank J. Zawadzki and the Princeton University Flow Cytometry Core facility for their assistance. All animal care and use conformed with institutional guidelines. Partially supported by NIH grants HL 50985, HL 46810, HL 52297, DK 38108, and F32HL09046 and the Medical Research Council, United Kingdom.

1 February 1995; accepted 26 April 1995

HERG, a Human Inward Rectifier in the Voltage-Gated Potassium Channel Family

Matthew C. Trudeau, Jeffrey W. Warmke,* Barry Ganetzky, Gail A. Robertson†

In contrast to other members of the Eag family of voltage-gated, outwardly rectifying potassium channels, the human *eag*-related gene (*HERG*) has now been shown to encode an inwardly rectifying potassium channel. The properties of HERG channels are consistent with the gating properties of Eag-related and other outwardly rectifying, S4-containing potassium channels, but with the addition of an inactivation mechanism that attenuates potassium efflux during depolarization. Because mutations in *HERG* cause a form of long-QT syndrome, these properties of HERG channel function may be critical to the maintenance of normal cardiac rhythmicity.

The *ether-à-go-go* (*eag*) gene was originally identified in *Drosophila* on the basis of its leg-shaking mutant phenotype (*1*), attributed to an increase in neuronal excitability and transmitter release at the neuromuscular junction (*2*). The polypeptide predicted by the sequence of the cloned gene exhibits the characteristic features of K^+ channels (*3*), and expression studies in frog oocytes confirm that *eag* encodes a functional K^+ channel (*4, 5*). The *eag* locus defines an extended gene family, with members falling into subfamilies on the basis of their sequence similarity: Eag, named for the original isolate from *Drosophila*; Elk, for *eag*-like K^+ channel; and Erg, for *eag*-related gene (*6*). Both *eag* and *M-EAG*, its mouse counterpart, encode voltage-gated, outwardly rectifying K^+ channels (*4, 5*). We report here that *HERG*, a gene in the Erg subfamily isolated from human hippocampus (*6*), encodes a K^+ channel with inwardly rectifying properties in spite of the extensive homology with the outwardly rectifying members of the Eag family (49% amino acid identity) (*7*).

Inward rectifiers are a large class of K^+-selective ion channels that preferentially conduct inward K^+ currents at voltages negative to the K^+ equilibrium potential (E_K). Their physiological roles are best understood in the heart, where their small outward conductances regulate the resting potential and contribute to the terminal phase of repolarization (*8*). At positive voltages they close, thus helping maintain the plateau of the action potential. In addition to the cardiac inward rectifier I_{K1}, the "delayed rectifier" I_{Kr}, which contributes substantially to the repolarization of the action potential, also exhibits profound inward rectification (*9*). Recent molecular characterization of inward rectifiers has focused on a family of channels sharing a hydropathy profile that predicts two transmembrane domains (*10*), in contrast to the six putative transmembrane domains in S4-containing channels of the Shaker (Sh) (*11*), Slowpoke (Slo) (*12*), and Eag (*6*) families.

We generated an expression construct for heterologous expression of *HERG* in frog oocytes from overlapping complementary DNAs (cDNAs) and a genomic fragment previously isolated from human DNA libraries (*13, 14*). A small inward current was sometimes seen after repolarization from a series of voltage steps (Fig. 1A). By comparison, oocytes expressing *M-EAG* have large outward currents under the same conditions (Fig. 1C). When oocytes injected with *HERG* cRNA were presented with hyperpolarizing voltage steps from 60 mV in elevated external K^+ concentration ($[K]_o$), large inward currents were observed (Fig. 1, D and E). HERG currents rapidly turned on and then declined with rates that were voltage-dependent. Currents evoked by stepping to −105 mV had a time-to-peak of 27 ± 4.6 ms (mean ± SD; $n = 7$). Current deactivation could be fitted with a biexponential function with time constants of 68.2 ± 6.6 ms and 292 ± 20.4 ms (mean ± SD; $n = 6$). The voltage range of activation of the inward HERG current shifted as $[K]_o$ was altered (Fig. 2A), as for inward rectifiers, with a Nernstian relation indicating K^+ selectivity (Fig. 2B).

M. C. Trudeau and G. A. Robertson, Department of Physiology, University of Wisconsin Medical School, 1300 University Avenue, Madison, WI 53706, USA.
J. W. Warmke and B. Ganetzky, Laboratory of Genetics, University of Wisconsin, Madison, WI, 53706, USA.
*Present address: Merck Research Laboratories, P.O. Box 2000, Rahway, NJ 07065, USA.
†To whom correspondence should be addressed.

HERG channels are blocked by relatively low concentrations of Cs^+ and Ba^{2+} (Fig. 3). The voltage-dependent block by Cs^+ is typical of inward rectifiers (*15*) and is interpreted to reflect Cs^+ entering the pore from the outside and interfering with K^+ permeation (Fig. 3A). Ba^{2+} inhibits the current with an inhibition constant (IC_{50}) of 0.6 mM, but apparently does not exhibit the voltage-dependent effects characteristic of other inward rectifiers (Fig. 3B).

Despite marked differences in the characteristics of HERG and M-EAG currents, the channels themselves have similar biophysical properties possibly related to shared structural features. The number of HERG channels available to conduct inward currents during a hyperpolarizing pulse is regulated by gating transitions that occur during a depolarizing prepulse (Fig. 4A). As the voltage of the prepulse was increased, the amplitude of HERG current during the subsequent hyperpolarization also increased. Corresponding gating transitions for M-EAG channels during depolarization are reflected in the instantaneous amplitudes of the deactivating tail currents (arrow in Fig. 4B). Such voltage-dependent gating behavior is a characteristic of most channels in the S4-containing superfamily and is generally attributed to the movement of charges in the S4 domain (*16*).

Standard models for gating in Sh (*17*) and other S4-containing channels are, with modification, consistent with the dual gating mechanisms we have observed in HERG channels. The impetus to invoke such models comes from the overall structural similarities of HERG with M-EAG and other S4-containing channels and from the work of Armstrong and colleagues showing that a delayed rectifier in squid axon could be transformed into an inward rectifier simply by the addition of an internal blocking particle (*18*). In those studies, sufficient concentrations of the blocker (for example, tetraethylammonium) inhibited outward currents, and the tail currents showed a time-dependent increase in amplitude reflecting the time course of alleviation of the block. We suggest that HERG inward currents may be similarly modified deactivation tail currents, with the time-dependent increase of the inward current reflecting the removal of a block or inactivation mechanism. A schematic for the model is as follows:

$$C_1 \rightleftarrows C_2 \rightleftarrows C_n \rightleftarrows O \rightleftarrows I(B)$$

At negative voltages, the channel is at rest in the closed state (C_1). Upon depolarization, it undergoes voltage-dependent conformational changes leading sequentially to the open state (O) and to the inactivated or blocked state [I(B)]. The forward rate for the $O \rightarrow I(B)$ transition must be very fast to account for the low levels of outward HERG current at the onset of depolarization. During subsequent hyperpolarization, the inactivation is alleviated and channels enter the O state, resulting in inward current flow. The current is transient as channels make the $O \rightarrow C_n$ transition (but at a slower rate than do M-EAG channels).

To extend the analogy between HERG and outwardly rectifying channels, we can describe the voltage dependence of the gating transitions during the depolarizing prepulse by fitting the relaxations of the subsequent currents as if they were deactivating tail currents and extrapolate to the moment the voltage was changed (inset in Fig. 4D). The resulting instantaneous current was normalized and plotted as a conductance (g/g_{max}) and is predicted to be proportional to the conductance at the voltage transition if the inward rectification [I(B)] were removed. The resulting plot is described by a Boltzmann with a voltage of half-maximal activation (V_o) of 6 mV and a slope of 11.7 mV per *e*-fold change in conductance ($n = 5$) (Fig. 4D). The corresponding values determined from M-EAG tail currents are −5 mV for V_o and a slope factor of 19 mV per *e*-fold change in conductance ($n = 6$). The gating transitions

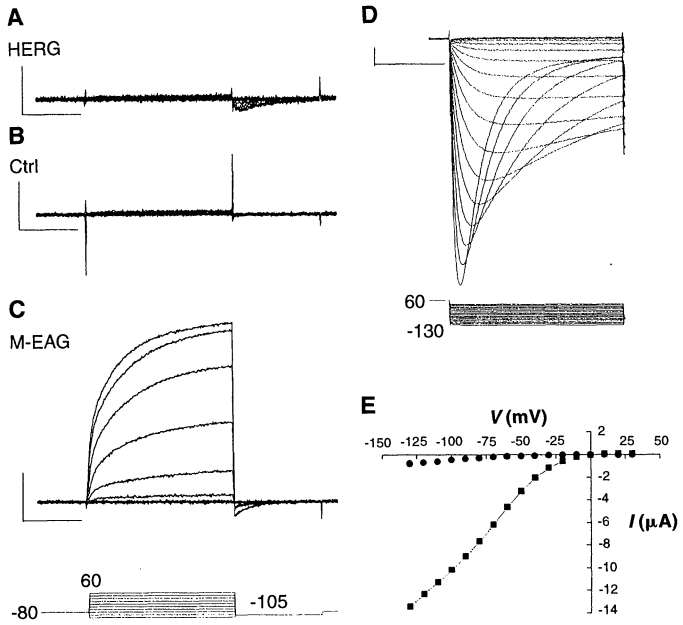

Fig. 1. Inwardly rectifying currents expressed in frog oocytes from the *HERG* cRNA measured with two-electrode voltage clamp. (**A**) Small inward currents are observed in oocytes expressing *HERG* in normal Ringer's subsequent to the series of voltage pulses. (**B**) Water-injected oocyte as a control (Ctrl) from the same oocyte batch as in (A). (**C**) Large outward currents recorded from oocyte expressing *M-EAG*. (**D**) Large inward currents evoked from same oocyte as in (A), but in high-K^+ Ringer's and with a different voltage command paradigm. The voltage was held at 60 mV for 200 ms before each voltage step shown. (**E**) *I-V* plot from oocyte in (D) (■) and from water-injected oocyte (●) from the same batch. Consistent results were obtained with $n > 50$ for HERG and $n = 21$ for water-injected oocytes. Electrodes contained 2 M KCl and had resistances between 0.5 and 1 megohm. Capacitive artifact (1 ms spike) was suppressed in (C) only, at the beginning and end of the voltage command. Currents in (A) to (C) were leak subtracted with the use of a linear leak protocol off-line (*29*). Bath solution for (A) to (C) was 96 mM NaCl, 2 mM KCl, 1.8 mM $CaCl_2$, 1.0 mM $MgCl_2$, 5 mM Hepes (pH 7.4) (normal Ringer's); bath solution for (D) was 100 mM KCl, 1.8 mM $CaCl_2$, 1.0 mM $MgCl_2$, 5 mM Hepes (pH 7.4) (high-K^+ Ringer's). Calibration, 1 μA and 100 ms.

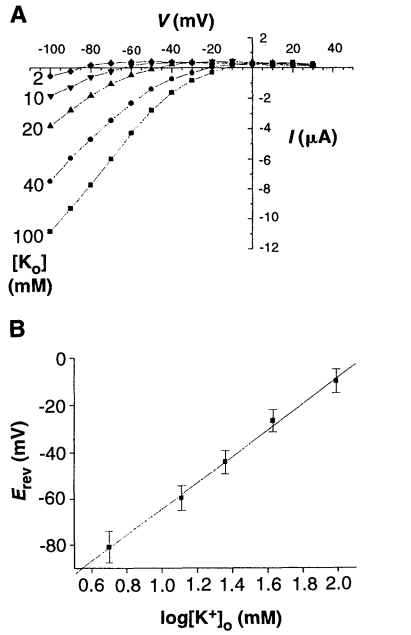

Fig. 2. Shift in HERG gating with changes in external K^+ concentration ($[K_o]$). (**A**) Typical peak *I-V* plot of HERG inward currents evoked under two-electrode voltage clamp. No leak subtraction was necessary. (**B**) Least-squares fit to mean reversal potential (E_{rev}) ± SD versus $\log[K]_o$ shows that $\Delta E_{rev} = 56$ mV per 10-fold change in $[K]_o$, consistent with a selectivity for K^+ over Na^+. E_{rev} is the voltage at 0 current for each *I-V* curve ($n = 5$). Bath solution was 100 mM [NaCl + KCl], 1.8 mM $CaCl_2$, 1.0 mM $MgCl_2$, 5 mM Hepes (pH 7.4).

during the depolarizing prepulse for HERG channels do not depend on $[K]_o$ (Fig. 4E), in contrast to the gating during the hyperpolarization, which exhibits a changing voltage dependence as a function of $[K]_o$ (Fig. 2A).

The time course of transitions into the I(B) state can be monitored indirectly by varying the duration of the depolarizing prepulse (Fig. 4F). According to the model, the amplitude of the extrapolated, instantaneous inward current should be proportional to the number of channels in the O and I(B) states at the end of the prepulse. If the O→ I(B) transition during depolarization is very fast, the time course of increase in the peak inward current amplitude should be determined by the rates of the transitions between the $C_1 \rightarrow O$ states, analogous to the rate of activation of Sh, M-EAG, and other outward rectifiers. The conductance measured in this way (from a holding potential of −100 mV) reaches steady-state with a half-time of 149 ± 1.7 ms (mean ± SD; $n = 5$).

These observations lead to the hypothesis that the S4 domain in HERG mediates conformational changes analogous to those leading to channel opening in related channels, with an inward rectification gate inhibiting K^+ efflux during depolarization. Inward rectification in HERG channels may arise from a soluble, internal blocking particle (*19*) such as Mg^{2+} or polyamines, which are proposed to compete with K^+ ions for binding sites along the conduction path of other inward rectifiers (*20*, *21*). Alternatively, the gate may be a rapidly induced form of the C-inactivation observed in Sh (*22*), or a peptide domain of the channel that provides an internal block by a ball-and-chain type mechanism (*17*).

KAT-1 channels from the plant *Arabidopsis* are inward rectifiers (*23*) with an S4 domain that senses the very negative voltages characteristic of plant cells (*24*). HERG and other Eag-related channels exhibit greater structural similarity to the KAT1 inward rectifier channel (~24% amino acid identity within the hydrophobic core) than to Sh-related channels (~15%) (*6*), and may share a similar structural basis for inward rectification.

A physiological role for HERG channels in regulating cardiac rhythmicity has been demonstrated by the recent discovery that the *HERG* gene is the locus for one form of long-QT syndrome (LQT-2) (*25*). This inherited disorder is characterized by a prolonged QT interval in the electrocardiogram arising from abnormally slow repolarization of action potentials (*26*). Individuals with LQT are at risk for sudden death from ventricular arrhythmia ("torsade de pointes"). The high levels of *HERG* expression in the heart (*25*) suggest that the electrophysiological phenotype of LQT-2 may be due directly to a mutational defect of HERG channels in cardiac cells. LQT syndrome also has been attributed to block of I_{Kr} by class III antiarrhythmic drugs (*27*), implicating HERG as a possible component of I_{Kr} channels. Indeed, when *HERG* expression is increased by 10-fold or more over levels used to study the inward component, an emerging outward component exhibits kinetics consistent with I_{Kr} (Fig. 4G). Furthermore,

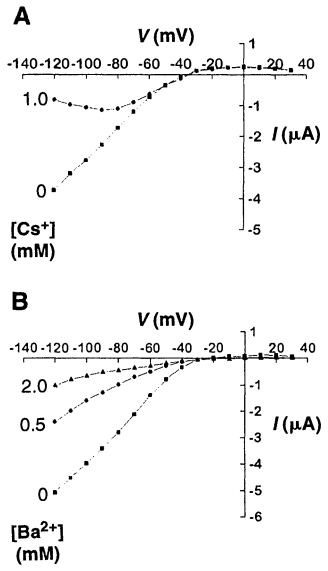

Fig. 3. Cs^+ and Ba^{2+} inhibit peak inward HERG current at low concentrations. (**A**) *I-V* plot of two-electrode voltage-clamp currents evoked before (■) and after (●) application of 1 mM Cs^+ the bath. Inhibition is more effective at more negative voltages ($n = 4$). (**B**) Ba^{2+} also inhibits current, but no voltage-dependent component is apparent over a range of concentrations ($n = 4$). No time dependence of cation block was observed, but this may have been masked by rapid decay of the inward currents. Bath solution was 20 mM KCl, 80 mM *N*-methyl glucamine chloride, 1.8 mM $CaCl_2$, 1.0 mM $MgCl_2$, 5 mM Hepes (pH 7.4).

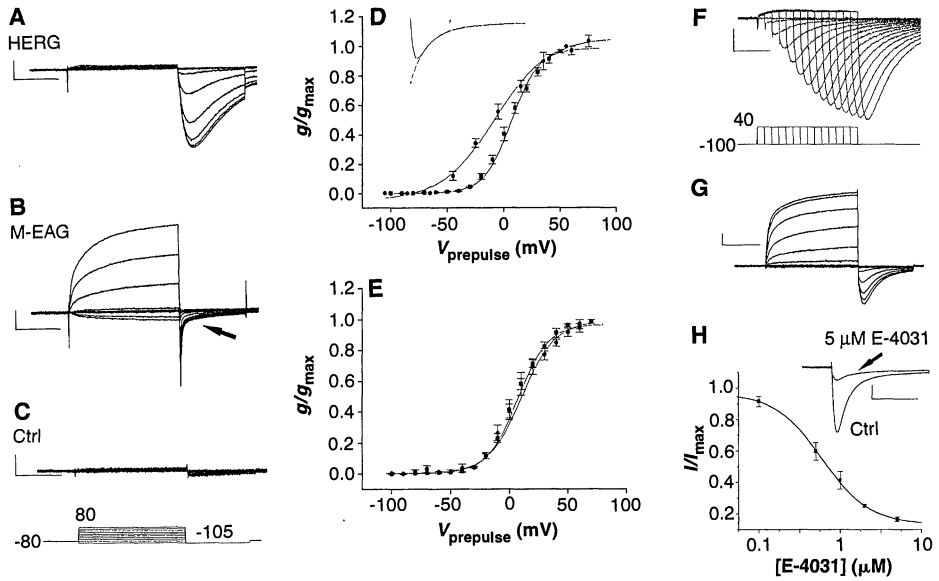

Fig. 4. Voltage-dependent gating and pharmacological block of HERG channels. A comparison of two-electrode voltage-clamp currents in high-K^+ Ringer's [100 mM KCl, 1.8 mM $CaCl_2$, 1.0 mM $MgCl_2$, 5 mM Hepes (pH 7.4)]. (**A**) HERG currents. (**B**) M-EAG currents. (**C**) Currents from water-injected oocyte. Oocytes in (A) and (C) were from the same frog. Calibration, 1 μA and 100 ms. (**D**) Equivalent *g-V* relations for M-EAG ($n = 6$) and HERG ($n = 5$). For M-EAG, instantaneous current values were determined from biexponential fits ($A_0 + A_1 e^{-t/\tau_1} + A_2 e^{-t/\tau_2}$) to deactivation tails [arrow in (B)] extrapolated to $t = 0$. For HERG, current relaxations were similarly treated as deactivation tails and fitted as shown in inset to (D) with the same biexponential function. The conductance was determined by normalizing instantaneous currents for M-EAG (●) and predicted instantaneous currents (in absence of inactivation) for HERG (■). (**E**) Voltage-dependent gating in HERG is independent of $[K]_o$. *g-V* relations evoked in 100 mM $[K]_o$ (■) and 20 mM $[K]_o$ (●) as described for (D). Solutions were as described, except for 20 mM $[K]_o$ containing 20 mM KCl and 80 mM NaCl. (**F**) Time course of voltage-dependent gating in HERG channels. Inward currents were evoked by hyperpolarizing commands (to −100 mV) after depolarizing prepulses (to 40 mV) of increasing duration. Capacitive spikes of 1-ms duration with each change in voltage were suppressed. (**G**) Outward currents observed with HERG expression at least 10 times that for previous experiments, as determined by the amplitude of the inward current in high-K^+ Ringer's (>100 μA; not shown) ($n = 12$). Solutions and voltage protocol are as in Fig. 1, A to C. (**H**) Dose-response curve showing inhibition of peak inward HERG current by E-4031. Currents were evoked by hyperpolarizing steps to −120 mV from a 60-mV prepulse; currents evoked in the presence of E-4031 were normalized to the current in the absence of drug ($n = 5$ oocytes, each tested at 0.1, 0.5, 1, 2, and 5 μM). Solution was high-K^+ Ringer's (as in Fig. 1D). (**Inset**) Block by 5 μM E-4031. Calibration, 1 μA and 100 ms.

the drug E-4031, which selectively blocks I_{Kr} (9), inhibits the inward HERG current with an IC_{50} of 588 nM (Fig. 4H), providing a pharmacological link between HERG and I_{Kr}. In contrast, the outward current is relatively resistant to E-4031. The selective sensitivity of the inward current, when the open probability of channels is presumed highest, suggests an open-channel block. The rectification mechanism that limits outward conductance may obstruct E-4031 access to the pore and may explain a recent report of E-4031 insensitivity in expressed HERG channels when an outward current protocol was used (*28*). These studies suggest that *HERG* encodes a component of I_{Kr}, but future studies will be necessary to determine the subunit composition and biophysical properties of native channels containing HERG subunits in human cardiac tissue.

REFERENCES AND NOTES

1. W. D. Kaplan and W. E. Trout, *Genetics* **61**, 399 (1969); nomenclature for genes and associated polypeptides is according to guidelines in *Trends in Genetics Guide to Genetic Nomenclature* (1995).
2. B. Ganetzky and C.-F. Wu, *J. Neurogenet.* **1**, 17 (1983).
3. J. W. Warmke, R. Drysdale, B. Ganetzky, *Science* **252**, 1560 (1991).
4. G. A. Robertson, J. W. Warmke, B. Ganetzky, *Biophys. J. Abstr.* **64**, A340 (1993).
5. A. Bruggemann, L. A. Pardo, W. Stuhmer, O. Pongs, *Nature* **365**, 445 (1993); J. Ludwig *et al.*, *EMBO J.* **13**, 4451 (1994).
6. J. W. Warmke and B. Ganetzky, *Proc. Natl. Acad. Sci. U.S.A.* **91**, 3438 (1994).
7. This work was previously reported in abstract form M. C. Trudeau, J. W. Warmke, B. Ganetzky, G. A. Robertson, *Biophys. J. Abstr.* **68**, A32 (1995); G. A. Robertson and M. C. Trudeau, *ibid.*, p. A363.
8. D. DiFrancesco and D. Noble, *Philos. Trans. R. Soc. London Ser. B* **307**, 353 (1985); G.-N. Tseng, D. Zipes and J. Jalife, Ed., *Cardiac Electrophysiology* (Saunders, Philadelphia, PA, ed. 2, 1995), pp. 260–268.
9. M. C. Sanguinetti and N. K. Jurkiewicz, *J. Gen. Physiol.* **96**, 195 (1990).
10. Y. Kubo, T. J. Baldwin, Y. N. Jan, L. Y. Jan, *Nature* **362**, 127 (1993); K. Ho *et al.*, *ibid.*, p. 31; F. Perier, C. M. Radeke, C. A. Vandenberg, *Proc. Natl. Acad. Sci. U.S.A.* **91**, 6240 (1994); E. N. Makhina, A. J. Kelly, A. N. Lopatin, R. W. Mercer, C. G. Nichols, *J. Biol. Chem.* **269**, 20468 (1994).
11. D. M. Papazian, T. L. Schwarz, B. L. Tempel, Y. N. Jan, L. Y. Jan, *Science* **237**, 749 (1987).
12. N. S. Atkinson, G. A. Robertson, B. Ganetzky, *ibid.* **253**, 551 (1991).
13. The *HERG* expression clone was constructed from three incomplete, overlapping gene fragments. One genomic and two cDNA clones (hh10 and hh1) were isolated as described (*6*). The cDNAs were ligated at a shared Sph I site, resulting in a clone containing all but the first 29 base pairs (bp) of the coding region. The 5′ coding region was added by means of three-way polymerase chain reaction (PCR) [O. Landt, H.-P. Grunert, U. Hahn, *Gene* **96**, 125 (1990)]. Primers were directed at the genomic clone to amplify a 76-bp segment containing the 5′ end of the coding region and a 47-bp overlap with the 5′ end of the hh10-1 fused cDNA. A Bam HI site was also added by means of the 5′ primer to facilitate subsequent manipulations. The product of this reaction was used as the 5′ primer in the next PCR with the hh10-1–fused cDNA as the template. The 3′ primer was complementary to sequence just downstream from a unique Nco I site in the hh10-1–fused cDNA. This reaction provided a 94-bp product containing the 5′ coding sequence from the genomic clone linked to the first 622 bp of the fused hh10-1 cDNA. This fragment included flanking Bam HI and Nco I sites, which were used to ligate the fragment to the pGH19 vector and the hh10-1–fused cDNA. The pGH19 expression vector is a modification of the pGEMHE vector [E. R. Liman, J. Tytgat, and J. P. Hess *Neuron* **9**, 861 (1992)].
14. Standard protocols for in vitro transcription, injection, and maintenance of oocytes were used [B. Rudy and L. E. Iverson, Eds., *Methods Enzymol.* **207**, 225–390 (1992)].
15. S. Hagiwara, S. Miyazaki, N. P. Rosenthal, *J. Gen. Physiol.* **67**, 612 (1976); S. Hagiwara, S. Miyazaki, W. Moody, J. Patlak, *J. Physiol.* **279**, 167 (1978).
16. W. Stuhmer *et al.*, *Nature* **339**, 597 (1989); D. Papazian, L. Timpe, Y. N. Jan, L. Y. Jan, *ibid.* **349**, 305 (1991); E. R. Liman, P. Hess, F. Weaver, G. Koren, *ibid.* **353**, 752 (1991).
17. T. Hoshi, W. N. Zagotta, R. W. Aldrich, *Science* **250**, 533 (1990).
18. C. M. Armstrong and L. Binstock, *J. Gen. Physiol.* **48**, 859 (1965); C. M. Armstrong, *ibid.* **54**, 553 (1969).
19. C. Vandenberg, *Proc. Natl. Acad. Sci. U.S.A.* **84**, 2560 (1987); H. Matsuda, A. Saigusa, H. Irisawa, *Nature* **325**, 156 (1987).
20. A. N. Lopatin, E. N. Makhina, C. G. Nichols, *Nature* **372**, 366 (1994).
21. E. Ficker, M. Taglialatela, B. A. Wible, C. M. Henley, A. M. Brown, *Science* **266**, 1068 (1994).
22. T. Hoshi, W. N. Zagotta, R. W. Aldrich, *Neuron* **7**, 547 (1991).
23. D. P. Schachtman, J. I. Schroeder, W. J. Lucas, J. A. Anderson, R. F. Gaber, *Science* **258**, 1654 (1992).
24. P. C. Zei, A. G. Miller, R. W. Aldrich, *Biophys. J. Abstr.* **68**, A32 (1995).
25. M. E. Curran *et al.*, *Cell* **80**, 795 (1995).
26. P. F. Cranefield and R. S. Aronson, in P. F. Cranefield, R. S. Aronson, Eds., *Cardiac Arrhythmias: The Role of Triggered Activity and Other Arrhythmias* (Futura, Mount Kisco, NY, 1988), pp. 553–579.
27. L. V. Buchanan, G. Kabell, M. N. Brunden, J. K. Gibson, *J. Cardiovasc. Pharmacol.* **22**, 540 (1993).
28. M. C. Sanguinetti, C. Jiang, M. E. Curran, M. T. Keating, *Cell* **81**, 299 (1995).
29. Linear leak was determined by stepping from −80 mV to −100 mV and −120 mV in solutions containing 10 mM or greater $[K]_o$. Under these conditions no conductance due to active currents could be measured (by direct observation or tail current analysis). Most records used for this study had leaks under these conditions of <2% peak currents and were therefore not leak subtracted.

30. We thank R. Fettiplace, M. Jackson, C. January, P. Lipton, P. Smith, and J. Wang for comments on the manuscript, E. Goulding and S. Siegelbaum for the pGH19 expression vector, and C. January for E-4031 and many helpful discussions. Supported by the American Heart Association of Wisconsin and the Wisconsin Alumni Research Foundation (G.A.R.) and by the NIH (B.G.) and the Muscular Dystrophy Association (J.W.W.).

27 March 1995; accepted 26 May 1995

Spatial Memory of Body Linear Displacement: What Is Being Stored?

Alain Berthoz, Isabelle Israël,* Pierre Georges-François, Renato Grasso, Toshihiro Tsuzuku

The ability to evaluate traveled distance is common to most animal species. Head trajectory in space is measured on the basis of the converging signals of the visual, vestibular, and somatosensory systems, together with efferent copies of motor commands. Recent evidence from human studies has shown that head trajectory in space can be stored in spatial memory. A fundamental question, however, remains unanswered: How is movement stored? In this study, humans who were asked to reproduce passive linear whole-body displacement distances while blindfolded were also able to reproduce velocity profiles. This finding suggests that a spatiotemporal dynamic pattern of motion is stored and can be retrieved with the use of vestibular and somesthetic cues.

Active or passive whole-body displacement is estimated by convergent signals from the vestibular system, vision, proprioception, and efferent copies of motor commands (*1*, *2*). The reconstruction of the experienced trajectory, called path integration (*3*), allows a return to the departure point, that is, homing (*3–5*). The term "integration" could correspond to the hypothesis that the brain computes distance either by cumulating successive positions along the path (*3*) or through temporal integration of velocity or acceleration. An alternate hypothesis is that the brain stores a spatiotemporal profile of motion and replays it during return.

Different species perform path integration in different ways. In humans, linear and angular passive whole-body displacements can be stored in spatial memory (*6*, *7*) and retrieved to generate accurate saccades to remembered targets (*8–11*); some cortical areas involved in this self-motion memory have been identified (*12*). Although the contribution of otoliths in small mammals has been debated (*4*, *13*), healthy humans can correctly estimate a linear distance after passive transport (*7*, *9*, *14*); this performance is degraded in the absence of the vestibular system, at least for small distances (*9*).

One main question, however, remains unanswered: How is movement stored? Is it

Laboratoire de Physiologie de la Perception et de l'Action, Collège de France–Centre National de la Recherche Scientifique (CNRS), 11 Place Mercelin Berthelot, 75006 Paris, France.

*To whom correspondence should be addressed.